Nondestructive quality assessment of longans using near infrared hyperspectral imaging

Woranitta Sahachairungrueng[1], Sontisuk Teerachaichayut[2]

(1. Department of Food Science, Faculty of Food-Industry, King Mongkut's Institute of Technology Ladkrabang, Bangkok 10520, Thailand; 2. Department of Food Process Engineering, Faculty of Food-Industry, King Mongkut's Institute of Technology Ladkrabang, Bangkok 10520, Thailand)

Abstract: Near infrared hyperspectral imaging (NIR-HSI) is a method that can be used to evaluate the quality of fruit nondestructively. The objective of this research was to study the feasibility of NIR-HSI reflectance mode, within the wavelength of 935-1720 nm, for predicting the quality of longans. The two important factors chosen were: total soluble solids (TSS) and moisture content (MC). Each longan was assessed by first measuring its spectral data then measuring its TSS and MC to establish calibration models using multiple linear regression (MLR) compared with partial least squares regression (PLSR). Original spectra of longans gave the optimum results by PLSR for developing the models with correlation coefficients (R_p) of 0.76 for TSS and 0.88 for MC as well as root mean square error of predictions (RMSEP) of 0.42% and 0.45% respectively. By image processing, the predictive images from the models for TSS and MC were created based on color scales. They showed different colors of longans related to the level of TSS and MC and the deviation in levels in different parts of each longan by the predictive image. The results showed it could be used for grading fruit giving NIR-HSI potential to be developed in on-line systems.

Keywords: spectra, nondestructive, calibration, prediction, images

Citation: Sahachairungrueng, W., and S. Teerachaichayut. 2022. Nondestructive quality assessment of longans using near infrared hyperspectral imaging. Agricultural Engineering International: CIGR Journal, 24 (1):217-227.

1 Introduction

Longan (*Dimocarpus longan* Lour.) is an important fruit in China, Vietnam, India, South Africa and many other countries, but particularly in Thailand where they are consumed mainly as fresh fruit for local and export markets and are also processed (Lin et al., 2020; Pholpho et al., 2011; and Wang et al., 2015). Longan is in high demand due to its delicious juicy aril that contains carbohydrates, protein, fiber, vitamin C, ascorbic acid and minerals (Yang et al., 2011; Yang and Chiang, 2019). Longan is a non-climacteric fruit that is a fruit that will not continue to ripen once it is removed from the tree, therefore will be little change in soluble solids concentration (SSC) after harvest (Jiang et al., 2002; Shi et al., 2016).

The codex standard for export of longans indicate that they must be good quality, no rots, not bruised and no obvious defects, practically free of any visible foreign matter, free of any foreign smell and/or taste, of suitable flavor for fresh consumption and are accepted of consumers (FAO/WHO, 2007). The external defects or unaccepted appearances of longans can be visually graded

Received date: 2020-11-08 **Accepted date:** 2021-06-08

***Corresponding author: Sontisuk Teerachaichayut,** Associate Professor, Department of Food Process Engineering, Faculty of Food-Industry, King Mongkut's Institute of Technology Ladkrabang, Chalongkrung Road, Ladkrabang, Bangkok 10520, Thailand. Email: sontisuk.te@kmitl.ac.th, Phone: +66-866047978.

by humans but important internal quality, such as taste and juicy flesh, based on their sweetness and moisture content cannot be determined by visual inspection. Therefore, a nondestructive method to evaluate the internal quality of longans would be a major asset for exporters.

Near infrared spectroscopy (NIRs) is a nondestructive technique that can be used for evaluating the qualities of various foods both qualitative and quantitative (Xue et al., 2013). NIRs can be applied in real-time on-line that is useful for commercial food processing lines (Roggo et al., 2007). Conventional NIRs scans only specific area of each sample and obtains spectral information of each sample that can be used representatively for analysis. However, defects and the chemical components of samples may not be homogenous over the whole area of each sample, which were reported for predicting nitrate level in intact pineapples (Srivichien et al., 2015), predicting translucent flesh disorder of mangosteens (Teerachaichayut et al., 2007) and hardening pericarp disorder in mangosteens (Teerachaichayut et al., 2011). Therefore, the conventional NIRs may not be the optimum method of assessing quality of fruit using data for spectral information at the specific area that is assumed to be representative of the whole fruit.

Hyperspectral imaging (HSI) is a technique that is used for assessing the qualities of various products, both quantitatively and qualitatively, by analyzing spectral information of each pixel from an image of a sample. It is non-destructive, fast, reliable, accurate and capable of use in real-time evaluation in on-line grading systems. NIR-HSI is a combination of spectroscopy that uses electromagnetic energy, near infrared and computer vision to evaluate digital images in a single system (Kamruzzaman et al., 2013). This technique allows both spatial and spectral data at the same time and can be used to analyze spectra at the single pixel level (Kamruzzaman et al., 2013; Caporaso et al., 2018). Therefore, spectral information from every pixel can be analyzed for the particular component, which can then be used as a comprehensive representation of its distribution within the sample. NIR-HSI has been successfully used in the analysis of some foods (Elmasry et al., 2012). There are many reports of this technique being used for example, determination and classification of shelf life for cakes (Sricharoonratana et al., 2021), detection internal browning levels of lychee pericarp (Yang et al., 2015), detection of blackspot in potatoes (Maestresalas et al., 2016), determination of sugar content in apple (Zhao et al., 2009), prediction of total soluble solids (TSS), titratable acidity (TA) and maturity index of limes (Teerachaichayut and Ho, 2017), assessment of TSS and pH in cherries (Li et al., 2018), assessment of the Haugh unit for freshness prediction of hens' eggs (Suktanarak and Teerachaichayut, 2017), prediction of texture and TSS in jelly (Onnom and Teerachaichayut, 2018), prediction of acidity and TSS in guavas (Klinbumrung and Teerachaichayut, 2018), prediction of moisture uniformity in mushroom slices and whole mushrooms (Lin et al., 2019), prediction of TSS in mushrooms (Xiao et al., 2020), assessment of firmness and TSS in sweet cherries (Pullanagari and Li, 2021), prediction of TSS of grapes (Benelli et al., 2021), assessment of moisture content in okra (Xuan et al., 2021) and predict adulteration in tapioca strarch (Khamsopha at al., 2021). NIR-HSI, therefore, has the potential to be used for evaluating the qualities of non-homogenous samples like foods or agricultural products. The objective of this research was therefore to use the NIR-HSI to analyze the qualities of longans in order to develop a non-destructive technique for predicting the internal qualities of longans that can be used for the on-line systems in grading and processing lines.

2 Materials and methods

2.1 Samples

Fresh longans cv. ‘Edo’ were purchased from the Suvarnabhumi market in Bangkok, Thailand. The experiment was conducted during the 2018 season. A set of 115 samples with the weight of 8.3-14.4 g, good appearance and without defects by visual inspection were selected for this study. Before measurement, samples were stored at 25°C in an air conditioning room for 24 h in order

to avoid the effect of temperature during the measurement.

2.2 NIR-HSI

As shown in Figure 1, each longan was laid on a moving scanner table of the instrument in a horizontal position where the top and bottom of each fruit were parallel to the floor. The scanning was applied using a NIR-HSI unit (Specim FX17e, Spectral Imaging Ltd., Oulu, Finland) with reflectance mode in the wavelength range of 935-1720 nm with 3.5 nm interval. The scanning speed and exposure time of the charge-coupled device (CCD) camera were 22.97 mm s^{-1} and 5.5 ms, respectively. White reference was scanned using the Teflon and dark reference was obtained at the closing state of the shutter unit for every measurement.

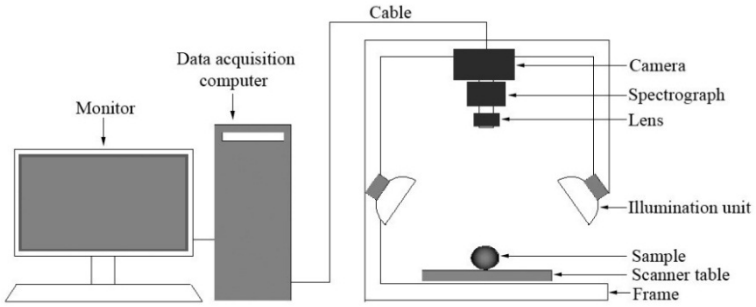

Figure 1 Schematic diagram of the instrument and sample presentation

2.3 Measurements

After scanning with the NIR-HSI, the peel and seed of each fruit were removed. Then, the flesh was chopped and squeezed. The following measurements were conducted:

Juice TSS: It was measured using a digital hand refractometer (PR 101, Palette Series, Atago Co., Ltd., Tokyo, Japan).

Flesh moisture content (MC): According to AOAC (2000), it was determined by removing the flesh from the peel and seed of each fruit, placing the flesh into an aluminum can and in a hot air oven (Binder, Model ED/FD, German) at 105°C for 2 hrs. The flesh was removed from the hot air oven and then put in the desiccator until it cooled to room ambient temperature. The flesh moisture content (w. b.) was calculated using the following Equation 1:

$$MC\ (\%) = \frac{(w_1 - w_2)}{w_1} \times 100 \qquad (1)$$

Where

w_1 = the mass of the sample before drying (g)

w_2 = the mass of the dried sample (g)

2.4 Image processing

The image of each measurement, scanned using the NIR-HSI unit, containing the spectral data of each sample and the background in the image. The spectral data of the background in each image had to be removed and only then the remaining spectral data of each sample as the region of interest (ROI) were used for analysis. The average spectrum from the ROI was used as a representative of each sample for developing the model. For establishing the calibration models TSS and MC were each a dependent variable and absorbance spectra in the wavelengths of 935-1720 nm (224 variables) were independent variables. The calibration model for each dependent variable was developed with the same procedure. Individual component and spectral data from the samples were divided into a calibration set and a prediction set.

The calibration models for each dependent variable were established by sampling the calibration set. Multiple linear regression (MLR) and partial least squares regression (PLSR) were compared in order to select the best method for establishing the models. Chemometric algorithms were investigated to improve the performance of the models. Spectral preprocessing methods such as smoothing methods (Savitzky-Golay), 1st Derivative, 2nd

Derivative, multiplicative scatter correction (MSC), standard normal variate (SNV) and combined methods were carried out in order to obtain the best model (Rinnan et al., 2009). The calibration model for each dependent variable from each spectral pretreatment was cross-validated. The best calibration model was selected by considering the lowest root mean square error of cross validation (RMSECV) and highest correlation coefficients (R_{cv}). The best calibration model was used to evaluate the accuracy for prediction by testing the model using samples in the prediction set. The accuracy of the calibration model was investigated by considering root mean square error of prediction (RMSEP) and correlation coefficients (R_p).

The calibration models for TSS and MC that had been acquired from the first step were used to create their predictive images. Each pixel of the sample's image contained spectral information. Therefore, each dependent variable or component (TSS and MC) in each pixel was predicted using each calibration model. The predicted value of the component was transferred to color using image processing (Juan de et al., 2009) where the range of each component was related to the color scale. Predictive images for each component were created and presented in colors based on the color scale which related to the predicted value of each component.

The Unscrambler software (CAMO, Osla, Norway) and the UmBio Evince hyperspectral image analysis software (Prediktera Evince, version 2.7.11, Sweden) were used for statistical analysis and image processing in this study.

3 Results and discussion

3.1 Absorbance spectrum

Due to the vibration energy of molecular bonds of components of the fruit is absorbed from NIR electromagnetic waves, therefore the absorbance peaks occur in the spectrum of the sample. The absorbance peaks may be the overtone vibrations of the molecular bonds between oxygen and hydrogen (O-H), carbon and hydrogen (C–H), nitrogen and hydrogen (N–H) or carbon and oxygen (C–O) (Williams and Norris, 1990). The original average absorbance spectrum of longans in the wavelength ranged 935-1720 nm is shown in Figure 2. The main peaks show the major absorption bands of water at around 1200 and 1450 nm that the overtone vibrations of the second overtones and the first overtones of OH stretching (Workman and Weyer, 2012). Water contains the molecular bonds of OH, and water is the main component of the fruit and in much higher quantity compared with other components in longans. Therefore, the absorbance peaks might be influenced from water that can cover all overlapped bands of the absorbance peaks of other components. Therefore, only two peaks, at around the water peaks, are clearly shown in the original spectrum of longan.

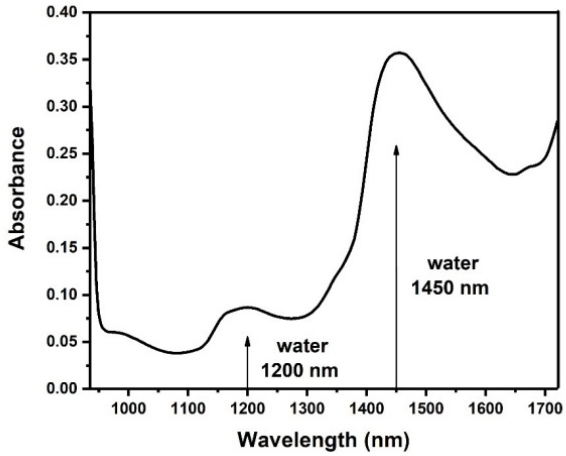

Figure 2 Average absorbance spectrum of longans

Teerachaichayut and Ho (2017) reported that the Savitzky-Golay 2nd derivative spectral pretreatment algorithm can be used to divide spectral peaks of components in samples. Therefore the 2nd derivative absorbance spectra of longans were investigated for TSS and MC (Figure 3). The absorption peaks for sugars showed at around 1450 nm due to molecules containing the first overtones of OH stretching (Workman and Weyer, 2012). Sucrose is the main component in the total sugar content in longan juice (Cheng et al., 2018) and showed the absorption peaks at 1196 and 1368 nm due to molecules containing the second overtones of CH stretching and the first overtones of OH stretching (Osborn et al., 1993, Workman and Weyer, 2012). Citric acid combined with water, showed absorption peaks at 960, 1420 and 1680 nm due to molecules containing the second overtones of OH stretching, the first overtones of OH stretching and the first overtones of CH_2 stretching (Subedi et. al., 2012). There were peaks of water at around 1154 and 1344 nm (Williams and Norris, 1990).

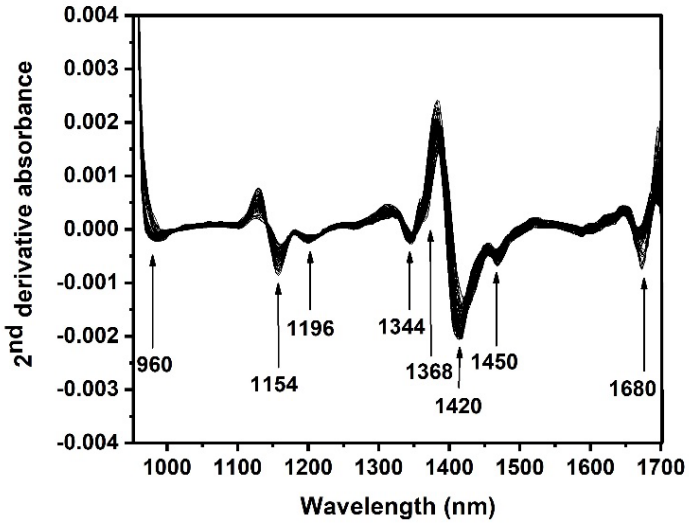

Figure 3 The 2nd derivative absorbance spectra of longans

3.2 Models for TSS and MC

Two groups of longans were used to establish calibration models for TSS and MC. Samples in each group (N=115) were divided into the calibration set (N=77) and the prediction set (N=38). In order to ensure the performance of the models in this study, the variation of the dependent variable in the calibration set and the prediction set was similar as well as maximum and minimum values of the dependent variable were set in the calibration set. The samples in the calibration set were used to establish and validate the calibration models for TSS and MC. Also, the samples in the prediction set were used to test the ability of the models. The characteristics of samples in the calibration set and the prediction set, used to establish models for TSS and MC, are given in Table 1.

Table 1 TSS and MC characteristics of longans in the calibration set and prediction set

Item	TSS		MC	
	Calibration set	Prediction set	Calibration set	Prediction set
Number	77	38	77	38
Range (%)	19.95-22.9	20.1-22.65	77.73-81.91	77.92-81.53
Mean (%)	21.32	21.39	79.64	79.66
SD	0.68	0.65	0.94	0.92

Note: SD = Standard deviation

MLR and PLSR were investigated in order to obtain the best models in this study. TSS and MC were used as the dependent variables while absorbance spectra were used as the independent variables. The absorbance spectra

at 960, 1154, 1196, 1344, 1368, 1420, 1450 and 1680 nm were used as independent variables for establishing the calibration models by MLR, while the whole spectra in the range 935-1720 nm were used for establishing the calibration models by PLSR. In order to create the best models for TSS and MC in this study, the performance of the calibration models by MLR and PLSR were compared. To select the optimal conditions for the best calibration models for TSS and MC, the various spectral pretreatment methods are investigated in the calibration sets for establishing the calibration models for TSS and MC as shown in Table 2.

Table 2 Performance of MLR models and PLSR models for TSS and MC

No.	spectral pretreatment	TSS						MC					
		MLR model			PLSR model			MLR model			PLSR model		
		N of Xi	R_{cv}	RMSECV (%)	Factors	R_{cv}	RMSECV (%)	N of Xi	R_{cv}	RMSECV (%)	Factors	R_{cv}	RMSECV (%)
1	Original	8	0.62	0.54	**2**	**0.77**	**0.44**	8	0.84	0.50	**3**	**0.86**	**0.47**
2	Smoothing	8	0.75	0.45	3	0.74	0.56	8	0.85	0.49	3	0.85	0.49
3	1st derivative	8	0.64	0.52	3	0.69	0.49	8	0.83	0.52	5	0.83	0.53
4	2nd derivative	8	0.61	0.54	2	0.70	0.48	8	0.72	0.65	8	0.74	0.64
5	MSC	8	0.64	0.53	3	0.66	0.52	8	0.83	0.52	2	0.85	0.50
6	SNV	8	0.62	0.54	3	0.66	0.51	8	0.84	0.50	2	0.85	0.48

Note: TSS = Total soluble solids

MC = Moisture content

MLR = Multiple linear regression

PLSR = Partial least squares regression

N = Number of samples

Xi = Independent variables

R_{cv} = Correlation coefficient of cross validation

RMSECV = Root mean square error of cross validation

MSC = multiplicative scatter correction

SNV = standard normal variate transformation

Results of cross-validation were considered in order to select the best models for TSS and MC. The results showed that PLSR models obtained better performance. For TSS, the original spectra of samples obtained the best results (R_{cv}= 0.77, RMSECV= 0.44%). For MC, the original spectra of samples also obtained the best results (R_{cv}= 0.86, RMSECV= 0.47%). Therefore, the original spectra were selected for developing the calibration models using PLSR for TSS and MC in this study.

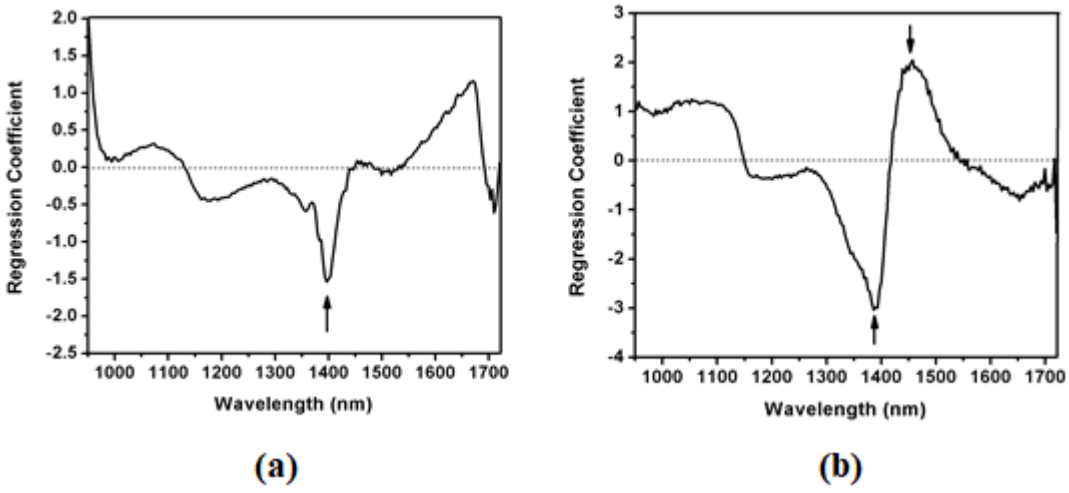

Figure 4 Regression coefficients of independent variables at various wavelengths of the PLSR models for TSS (a) and MC (b)

In Figure 4, the highest absolute values of regression coefficient of the PLSR models for TSS and MC in the

wavelength range of 935-1720 nm are around 1400-1450 nm, which are due to the first overtone vibrations of OH stretching (Williams and Norris, 1990).

To evaluate the accuracy of the calibration models for TSS and MC, the samples in the prediction sets were used for testing the models. The results of evaluating the models for TSS and MC by the samples in the prediction sets are shown in Table 3. The model for TSS obtained R_p of 0.76 and RMSEP of 0.42%. The model for MC obtained R_p of 0.88 and RMSEP of 0.45%.

Table 3 The results of the PLSR models for TSS and MC

Pre-treatment		TSS	MC
		original	original
Factors		2	3
Calibration set	N	77	77
	R_c	0.78	0.88
	RMSEC (%)	0.42	0.44
Prediction set	N	38	38
	R_p	0.76	0.88
	RMSEP (%)	0.42	0.45

Note: TSS = Total soluble solids

MC = Moisture content

N = Number of samples

R_c = correlation coefficients of calibration

RMSEC = root mean square error of calibration

R_p = correlation coefficients of prediction

RMSEP = root mean square error of prediction

The scatter plots of actual values versus predicted values of the two qualities of longans are shown in Figure 5. A 45-degree line was a perfect fit and was therefore used as a reference for comparing the performance of the model in prediction. The good accuracy for prediction could be seen from the scatter plot that was close to the 45-degree line. The results of accuracy based on the scatter plots for TSS and MC were shown in Figure 5a and 5b, respectively.

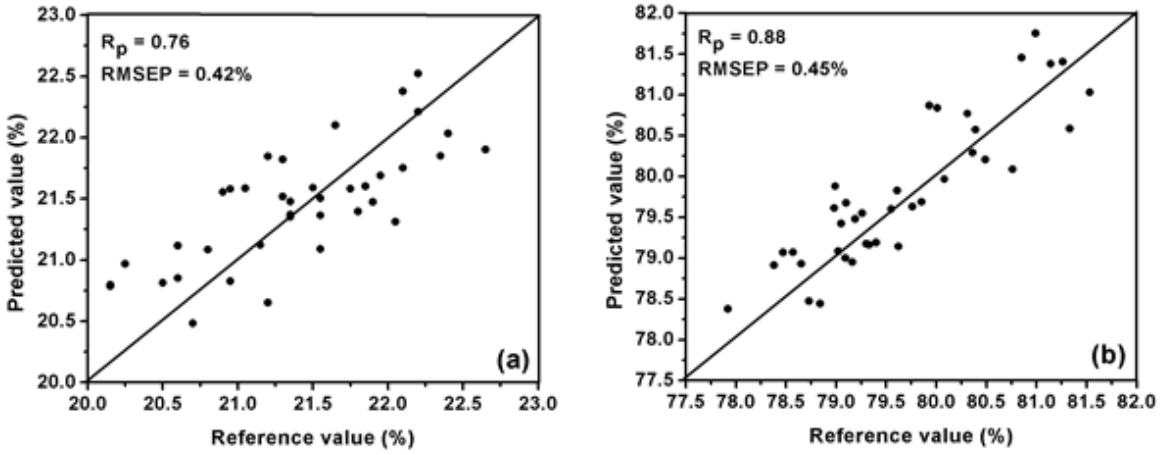

Figure 5 Scatter plots of actual and predicted values for TSS (a) and MC (b)

3.3 Quality prediction images

Each pixel in the image of each longan contained spectral data that were acquired by NIR-HSI. Spectral data in each pixel could be used as the independent variables for predicting the dependent variables by the models.

Therefore, each pixel of the image could be used as a predictor of TSS and MC from the calibration models.

In order to present the value of dependent variables in each pixel, the colors were interpreted from the value of dependent variables using the color scale from the image processing. The colors could be applied on an individual pixel in the whole fruit and the quality prediction images could be presented, as previously reported by Teerachaichayut and Ho (2017). The acquired color images, where the attractive features enabled the presentation of the quality information of longans in each pixel by visualization, which were the color scales for TSS and MC. Therefore, the colors in the images showed the level and distribution of components in the fruit. The acquired prediction images were presented based on the color scales that were related to the level of each component. The color scale in this study was defined from red to blue conforming with high to low values of TSS and MC. The prediction images of longans with various TSS and MC as well as the average prediction values for each sample are shown in Figure 6 and Figure 7, respectively.

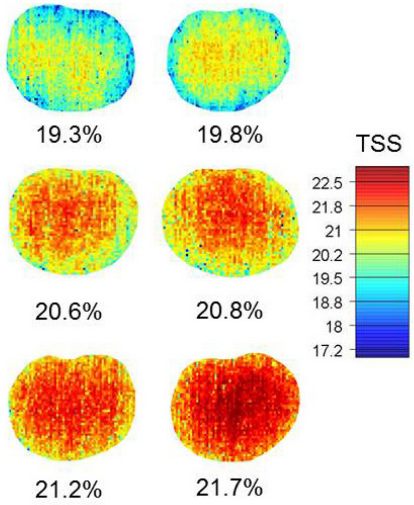

Figure 6 The prediction images and average prediction values of TSS in longans

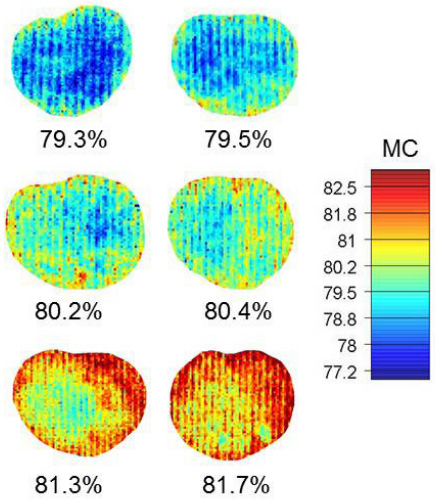

Figure 7 The prediction images and average prediction values of MC in longans

For the prediction images for TSS and MC of longans, each image showed a distribution of color in different parts of the fruit, indicating that TSS and MC weren't homogeneous in the fruit. However, for classifying the whole longans for TSS and MC by the prediction images, the colors were clearly related differently for their TSS and

MC values indicating that their levels in whole longans could be classified by using the quantity of blue, light blue, yellow and red, based on the color scale that presented blue for lowest level and red for the highest level. The results showed that the qualities of longans could be nondestructively graded by visual inspection using prediction images. Therefore, the visualization of longans for predicting the quantity of TSS and MC were shown to be possible using NIR-HSI.

4 Conclusion

Intact longans were scanned by reflectance NIR-HSI in order to test if they could be applied nondestructively to determine their quality. The best calibration models for TSS and MC were established using original spectra in the wavelength of 935-1720 nm by PLSR. The prediction images of longans for TSS and MC were successfully created by interpreting colors in each pixel based on the color scales. These colors varied in each fruit meant components in each fruit weren't homogeneous. From this it was concluded that the prediction images could be used for classifying the qualities of longans by visualization. This means that NIR-HSI has the possibility of being applied to predict TSS and MC in longans, giving it the potential for application in on-line grading systems.

Acknowledgements

The authors would like to thank the Faculty of Food-Industry, King Mongkut's Institute of Technology Ladkrabang, Thailand for the research fund (No. 2562-01-07002) and be grateful to Prof. Panmanas Sirisomboon for technical help as well as Prof. A. K. Thompson for editing English language and revision of this manuscript.

References

AOAC. 2000. *Official Methods of Analysis of AOAC International*. **17th ed**. Gaithersburg, MD, USA: Association of Analytical Communities.

Benelli, A., C. Chiara, L. Rugni, and A. Fabbri. 2021. In-field and non-destructive monitoring of grapes maturity by hyperspectral imaging. *Biosystems Engineering*, 207(7): 59-67.

Caporaso, N., M. B. Whitworth, S. Grebby, and I. D. Fisk. 2018. Non-destructive analysis of sucrose, caffeine and trigonelline on single green coffee beans by hyperspectral imaging. *Food Research International,* 106: 193-203.

Cheng, Y., H. Lan, L. Zhao, K. Wang, and Z. Hu. 2018. Characterization and prebiotic potential of longan juice obtained by enzymatic conversion of constituent sucrose into fructo-oligosaccharides. *Molecules,* 23(10): 1-13.

Elmasry, G., M. Kamruzzaman, D. W. Sun, and P. Allen. 2012. Principles and applications of hyperspectral imaging in quality evaluation of Agro-food products: A review. *Critical Reviews in Food Science and Nutrition,* 52(11): 999-1023.

FAO/WHO. 2007. *Fresh Fruits and Vegetables.* **1st ed**. Rome, Italy: The Secretary Codex Alimentarius Commission.

Jiang Y., Z. Zhang, D. C. Joyce, and S. Ketsa. 2002. Postharvest biology and handling of longan fruit (*Dimocarpus longan Lour.*). *Postharvest Biology and Technology*, 26(3): 241-252.

Juan de, A., M. Maeder, T. Hacewicz, L. Duponchel, and R. Tauler. 2009. Chemometric tools for image analysis. In *Infrared and Raman Spectroscopic Imaging,* eds. R. Salzer, and H. W. Siesler, 65-112. Weinheim, Germany: Wiley-VCH,.

Kamruzzaman, M., D. Sun, G. Elmasry, and P. Allen. 2013. Fast detection and visualization of minced lamb meat adulteration using NIR hyperspectral imaging and multivariate image analysis. *Talanta,* 103: 130-136.

Khamsopha, D., W. Sahachairungrueng, and S. Teerachaichayut. 2021. Utilizing near infrared hyperspectral imaging for quantitatively predicting adulteration in tapioca starch. *Food Control*, 123(6): 107781.

Klinbumrung, N., and S. Teerachaichayut. 2018. Quantification of acidity and total soluble solids in guavas by near infrared hyperspectral imaging. In *Proc. 4th International Conference on Green Design and Manufacture 2018, AIP Conference Proceedings 2030*, 020209-1–020209-5, Ho Chi Minh, Vietnam, 29–30 April 2018.

Li, X., Y. Wei, J. Xu, X. Feng, F. Wu, R. Zhou, J. Jin, K. Xu, X. Yu, and Y. He. 2018. SSC and pH for sweet assessment and maturity classification of harvested cherry fruit based on NIR hyperspectral imaging technology. *Postharvest Biology and Technology*, 143: 112-118.

Lin, X., J. Xu, and D. Sun. 2019. Investigation of moisture content uniformity of microwave-vacuum dried mushroom (Agaricus bisporus) by NIR hyperspectral imaging. *LWT - Food Science and Technology,* 109: 108-117.

Lin, Y., N. Li, H. Lin, M. Lin, Y. Chen, H. Wang, M. A. Ritenour, and Y. Lin. 2020. Effects of chitosan treatment on the storability and quality properties of longan fruit during storage. *Food Chemistry,* 306(5): 125627.

Maestresalas, A. L., J. C. Keresztes, M. Goodarzi, S. Arazuri, C. Jaren, and W. Saeys. 2016. Non-destructive detection of blackspot in potatoes by Vis-NIR and SWIR hyperspectral imaging. *Food Control,* 70: 229-241.

Onnom, P., and S. Teerachaichayut. 2018. Development of calibration models to predict texture and total soluble solids in jelly using hyperspectral imaging. *In Proc. 4th International Conference on Green Design and Manufacture 2018*, *AIP Conference Proceedings 2030*, 020211-1-020211-5, Ho Chi Minh, Vietnam, 29–30 April 2018.

Osborne, B. G., T. Fearn, and P. H. Hindle. 1993. *Practical NIR Spectroscopy: With Applications in Food and Beverage Analysis*. Harlow, UK: Longman Scientific and Technical.

Pholpho, T., S. Pathaveerat, and P. Sirisomboon. 2011. Classification of longan fruit bruising using visible spectroscopy. *Journal of Food Engineering,* 104(1): 169-172.

Pullanagari, R. R., and M. Li. 2021. Uncertainty assessment for firmness and total soluble solids of sweet cherries using hyperspectral imaging and multivariate statistics. *Journal of Food Engineering*, 289(11–12): 110177.

Rinnan, A., F. V. D. Berg, and S. B. Engelsen. 2009. Review of the most common pre-processing techniques for near-infrared spectra. *Trends in Analytical Chemistry,* 28(10): 1201-1222.

Roggo, Y., P. Chalus, L. Maurer, C. Lemamartinez, A. Edmond, and N. Jent. 2007. A review of near infrared spectroscopy and chemometrics in pharmaceutical technologies. *Journal of Pharmaceutical and Biomedical Analysis*, 44(3): 683-700.

Shi, S., W. Wang, L. Liu, B. Shu, Y. Wei, D. Jue, J. Fu, J. Xie, and C. Liu. 2016. Physico-chemical properties of longan fruit during development and ripening. *Scientia Horticulturae,* 207:160-167.

Sricharoonratana, M., A. K. Thompson, and S. Teerachaichayut. 2021. Use of near infrared hyperspectral imaging as a nondestructive method of determining and classifying shelf life of cakes. *LWT - Food Science and Technology*, 136(part2): 110369.

Srivichien, S., A. Terdwongworakul, and S. Teerachaichayut. 2015. Quantitative prediction of nitrate level in intact pineapple using Vis–NIRS. *Journal of Food Engineering,* 150: 29–34.

Subedi, P. P., K. B. Walsha, and D. W. Hopkins. 2012. Assessment of titratable acidity in fruit using short wave near infrared spectroscopy. Part A: establishing a detection limit based on model solutions. *Journal of Near Infrared Spectroscopy,* 20(4): 449–457.

Suktanarak, S., and S. Teerachaichayut. 2017. Non-destructive quality assessment of hens' eggs using hyperspectral images. *Journal of Food Engineering,* 215: 97-103.

Teerachaichayut, S., K. Y. Kil, A. Terdwongworakul, W. Thanapase, and Y. Nakanishi. 2007. Non-destructive prediction of translucent flesh disorder in intact mangosteen by short wavelength near infrared spectroscopy. *Postharvest Biology and Technology,* 43(2): 202–206.

Teerachaichayut, S., A. Terdwongworakul, W. Thanapase, and K. Kiji. 2011. Non-destructive prediction of hardening pericarp disorder in intact mangosteen by near infrared transmittance spectroscopy. *Journal of Food Engineering,* 106(3): 206–211.

Teerachaichayut, S., and H. T. Ho. 2017. Non-destructive prediction of total soluble solids, titratable acidity and maturity index of limes by near infrared hyperspectral imaging. *Postharvest Biology and Technology,* 133: 20-25.

Wang, B., H. Tan, W. Fang, L. W. Meinhardt, S. Mischke, T. Matsumoto, and D. Zhang. 2015. Developing single nucleotide polymorphism (SNP) markers from transcriptome sequences for identification of longan (*Dimocarpus longan*) germplasm. *Horticulture Research,* 2(1): 14065.

Williams, P., and K. Norris. 1990. *Near-Infrared Technology in the Agriculture and Food Industries.* St Paul, Minnesota: American Association of Cereal Chemists, Inc.

Workman, J., and L. Weyer. 2012. *Practical Guide and Spectral Atlas for Interpretive Near-Infrared Spectroscopy.* **2nd ed.** USA: Taylor and Francis Group, LLC.

Xiao, K., Q. Liu. L. Wang, B. Zhang, W. Zhang, W. Yang, Q. Hu, and F. Pei. 2020. Prediction of soluble solid content of Agaricus bisporus during ultrasound-assisted osmotic dehydration based on hyperspectral imaging. *LWT - Food Science and Technoogy.,* 122(6): 109030.

Xuan, G., C. Gao, Y. Shao, X. Wang, Y. Wang, and K. Wang. 2021. Maturity determination at harvest and spatial assessment of

moisture content in okra using Vis-NIR hyperspectral imaging. *Postharvest Biology and Technology*, 180(5): 111597.

Xue, J., S. Zhang, H. Sun, and J. Zhou. 2013. Study of Malus Asiatica Nakai's firmness during different shelf lives based on visible/near-infrared spectroscopy. *Mathematical and Computer Modelling,* 58(11-12): 1829-1836.

Yang, B., Y. Jiang, J. Shi, F. Chen, and M. Ashraf. 2011. Extraction and pharmacological properties of bioactive compounds from longan (*Dimocarpus longan* Lour.) fruit – A review. *Food Research International,* 44(7): 1837-1842.

Yang, C., D. Sun, and N. Wand. 2015. Rapid detection of browning levels of lychee pericarp as affected by moisture contents using hyperspectral imaging. *Computers and Electronics in Agriculture*, 113: 203-212.

Yang, M., and P. Y. Chiang. 2019. Effects of smoking process on the aroma characteristics and sensory qualities of dried longan. *Food Chemistry,* 287(11): 133-138.

Zhao, W., V. Saritporn, Q. Chen, C. Sumpun, and C. Rachata. 2009. Nondestructive measurement of sugar content of apple using hyperspectral imaging technique. *Maejo International Journal of Science and Technology*, 3(1): 130-142.